Proceedings of the 2018 IISE Annual Conference
K. Barker, D. Berry, C. Rainwater, eds.

Ultrasound-Assisted Manipulation of Micro-particles in Fluid Matrix to Create Highly Aligned Anisotropic Composite Structures

Parth Chansoria[1], Omid Yousefian[2], Marie Muller[2,3], Rohan A. Shirwaiker[1, 3*]
[1]Edward P. Fitts Department of Industrial & Systems Engineering, [2] Department of Mechanical & Aerospace Engineering, [3]UNC-NCSU Joint Department of Biomedical Engineering, North Carolina State University, Raleigh, North Carolina 27695.
* Email: rashirwaiker@ncsu.edu

Abstract

Structural anisotropy, often observed in naturally occurring materials such as wood and human tissues, is central to the function in several engineered and non-engineered applications. In this study, we present the theory and proof-of-concept demonstration of an ultrasound-assisted non-contact manufacturing approach to create well-defined spatial patterns of micro-particles within a fluid matrix. A chamber with opposing pair of ultrasonic transducers was designed and prototyped based on standing bulk acoustic wave theory, and it was used to study the effects of ultrasound frequency (1, 1.5, 2, 3 MHz) and voltage amplitude (80, 160 mVpp) on alignment characteristics of polymer micro-particles (mean Ø = 8 μm) suspended in water (0.01 g/ml). The experimental results were consistent with theory in that the micro-particles aligned along linear strands, with the inter-strand spacing reducing with increasing frequency ($p < 0.05$). Increasing voltage amplitude reduced the time taken to align the particles, but it did not significantly change the observed spacing ($p > 0.05$). The observed spacing, however, was higher than the theoretical spacing of half-wavelength, for each frequency and amplitude. The alignment of living human adipose derived stem cells in viscous alginate hydrogel matrix was also successfully demonstrated. The approach presented herein can be scaled up into manufacturing processes, including layered manufacturing, to create highly functional mechanically and/or electrically anisotropic composites through controlled spatial geometry, as well as to biofabricate engineered tissues with aligned cells and extracellular matrix components to mimic natural tissues.

Keywords
Ultrasound, bulk acoustic wave, acoustic radiation force, anisotropic alignment, biofabrication

1. Introduction

Material anisotropy is at the very essence of physical design of natural objects. By varying the material composition along different directions, and/or incorporating complex arrangement of cells and other constituents [1, 2], these objects exhibit desired mechanical loading and energy absorption characteristics, whilst conserving space for other essential functions such as material transport. Hardwood, like Balsa for example, is characterized by densely packed honeycomb arrangement of fiber cells providing the structural support, with interspersed large spacious vessels for nutrient transport through the honeycombs also adding to the bending strength [1]. Many human tissues also demonstrate such anisotropy in the organization of their cells and extracellular matrix (ECM) fibers, which is central to their primary functions in the body [3]. For example, the cells and ECM collagen fibers of ligaments and tendons, which primarily experience uniaxial tensile loads, are generally well-aligned uniaxially along the direction of tensile loading [4].

The concepts entailing material anisotropy have been used to create engineered structures with superior mechanical characteristics [5, 6]. For example, lightweight fiber reinforced composites demonstrating high strength or stiffness are well established [7]. However, creation of complex anisotropic structures can be challenging. Here, layer based manufacturing, including 3-D printing, has emerged as a valuable tool to create complex shapes, with both polymers and metals processing capabilities [8]. Several advances have recently been made wherein polymer composites have been tailored for layered manufacturing techniques, while delivering good mechanical characteristics [9, 10]. Although adding reinforcements improves the strength and stiffness of the material, higher concentrations are often associated with increased brittleness and viscosity, which leads to difficulty in manipulating the material, especially

in layered manufacturing or injection molding. In tissue engineering applications which involve manipulation of living cells within viscous hydrogels, shear force on cells, which increases due to increased pressures needed to extrude such hydrogels, is one of the biggest causes of cell death [11, 12].

This study presents a new non-contact manufacturing approach for patterning reinforcements in fluid matrices to create highly anisotropic composite constructs, while overcoming drawbacks of existing methods. A proof of concept has been demonstrated, wherein spherical micro-particles suspended in water are aligned into linear patterns using acoustic radiation forces from an ultrasonic standing wave. The standing wave is generated from the interference of longitudinal bulk acoustic waves (BAW), generated from an opposing pair of ultrasonic piezo-transducers, propagating across the fluid (Figure 1). The toner particles suspended within water slowly migrate to the nearest pressure node, acted upon by the ensuing acoustic radiation forces. These pressure nodes, along which the particles aggregate, are planes parallel to the walls of the transducers. As seen from the top, the particle clusters appear as linear strands, uniformly separated by half the wavelength of the ultrasound, in theory (Figure 1b). This study characterizes the effects of ultrasound frequency and pressure amplitude (governed by voltage applied to the transducers) on the alignment characteristics of the micro-particles.

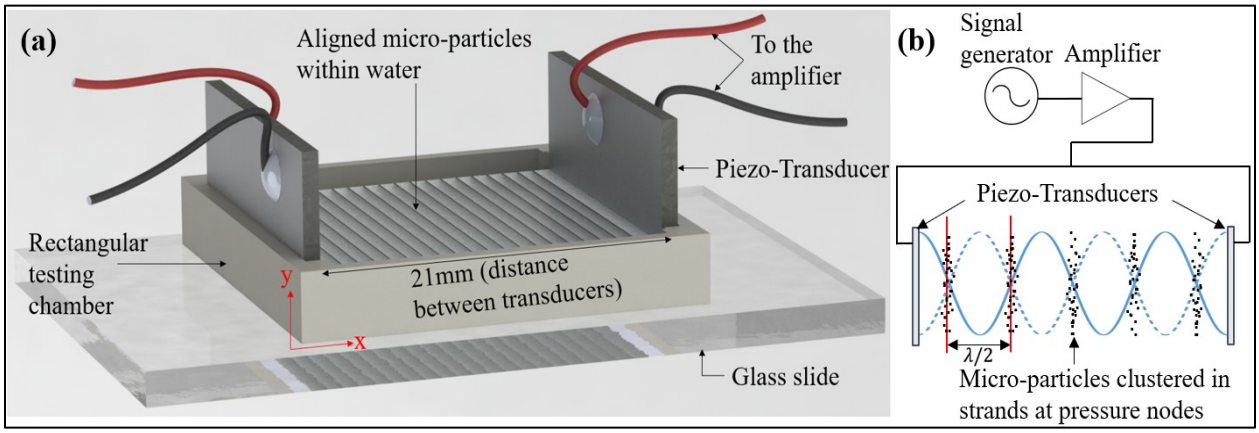

Figure 1: (a) Ultrasound-assisted manipulation testing fixture schematic, and (b) Circuitry to excite the transducer setup in parallel at a particular frequency and voltage amplitude.

2. Fundamentals of Acoustic Manipulation of Particles

The physics associated with the acoustic manipulation of particles via standing BAW is presented in this section. The pressure distribution within the standing BAW in the matrix, and the resulting pressure-driven radiation force on a particle within the fluid are discussed. This acoustic radiation force (ARF) tends to move the particle to the nearest pressure node and must overcome the fluid resistive force. The magnitude of the resistive force dictates the minimum theoretical ARF necessary to move the particle, and is governed by the instantaneous particle velocity and acceleration in each longitudinal wave component of the standing wave.

2.1 Acoustic Pressure Field in a Standing Wave:

In response to the applied signal, the piezo-transducers (Figure 1) vibrate along their thicknesses at resonant frequency, causing a longitudinal BAW to emanate along the X-axis from each transducer. For an opposing pair of transducers, the pressure variation in the resulting standing wave in fluid [13] along the X-axis is given by Equation (1).

$$p(x,t) = P_o Cos(\omega t) Cos(kx) \tag{1}$$

where '$p(x,t)$' is the acoustic pressure, 'c' is the longitudinal wave speed, 'P_o' is the pressure amplitude, '$\omega = 2\pi f$' is the angular velocity, 'f' is the ultrasound frequency, and '$k = \omega/c$' is the wave number. The wave number is related to the separation 'L' between the transducers (Equation (2)). After substituting '$c = \lambda/f$' in Equation (1), the separation between the transducers is determined to be an integer multiple of half the wavelength of ultrasound (λ) in order for a standing wave to be created (Equation (3)).

$$k = n\pi/L \tag{2}$$

$$L = n\lambda/2 \tag{3}$$

2.2 Acoustic Radiation Forces:

For a standing acoustic pressure field in a medium, the ARF on a particle suspended in the medium between any two pressure nodes is given by the time averaged effect of the pressure variation and its associated momentum flux between the nodes [14] over the entire surface area of the particle. This ARF pushes the particle towards the nearest pressure node. Now, the micro-particles used in this study (mean Ø 8 µm) are an order of magnitude larger than the viscous penetration depth (0.6 µm) [14] and several orders of magnitude less than the wavelength ($r << \lambda$) [14] at 1 MHz frequency in water at room temperature. Hence, the ARF can be determined using the inviscid theory [14], which, for a standing wave in a rectangular testing chamber with parallel walls at x=0 and x=L, is given by Equation (4).

$$F_{rad} = (\pi/3)(k_l - k_p)r^3(2\pi/\lambda)P_o^2 Sin(4\pi x/\lambda) \quad (4)$$

This is a simplified expression of the ARF considering near buoyant particles [14] (density ~1g/cm^3), where r is the particle radius, k_l is the fluid compressibility, k_P is the particle compressibility and P_o is the pressure amplitude.

2.3 Fluid Resistive Forces:

When the particles, are migrating towards the nearest pressure node, they experience fluid resistive forces given by Equation (5).

$$F_{resist} = 6\pi\mu Rv + (4\pi R^3/3)\rho_l a/2 \quad (5)$$

Where μ is the dynamic viscosity of water, ρ_l is the density of water, and v and a are the instantaneous velocity and acceleration of the particle respectively. The first term on the right denotes the viscous drag on the particle, while the second term denotes the resistance due to the inertia of the accelerating particle.

2.4 Instantaneous Particle Acceleration and Velocity:

Euler's equation (Equation (6)) can be used to derive the instantaneous acceleration (Equation (7)) and velocity (Equation (8)) by neglecting second order terms and assuming that the particle moves with the fluid momentum flux.

$$\rho_l \partial v/\partial t = -\partial p/\partial x \quad (6)$$

$$a = \partial v/\partial t = (P_o/\rho_l)(2\pi/\lambda)Sin(2\pi x/\lambda)Cos(\omega t) \quad (7)$$

$$v = (P_o/\rho_l)(2\pi/\lambda)(1/\omega)Sin(2\pi x/\lambda)Sin(\omega t) \quad (8)$$

Based on Equations (5), (7) and (8), the minimum ARF that would be required to move the particle to the nearest node can be estimated. This has been further addressed in the results and discussion section.

3. Experimental Materials and Methods

3.1 Preparation of Micro-particle Suspension

Polyethylene toner particles (mean Ø 8 µm) extracted from an inkjet printer cartridge were suspended within deionized (DI) water. In order to reduce the hydrophobicity of the micro-particles and create a homogenous suspension at a concentration of 0.01 g/ml, 100 µl of Tween-20 surfactant was added to 50 ml of DI water at 80°C. After the solution cooled to room temperature, 0.5 g of toner particles were added and the solution gently stirred.

3.2 Design and Fabrication of Ultrasound Actuation Setup

A schematic of the setup is shown in Figure 1. Pairs of Lead-Zirconium-Titanate Piezo transducers (PZT-4, Steiner & Martins Inc.), each having thickness mode resonant frequency (1 MHz, 1.5 MHz, 2 MHz or 3 MHz), were bonded onto the opposite walls of a 3D printed testing chamber, with a separation distance of 21 mm between the opposing transducers. This distance is an integer multiple of half the wavelength (Equation (3)) for all four frequencies, assuming the speed of sound in DI water to be 1500 m/s at 20°C. To complete the testing chamber assembly to contain the micro-particle suspension in between the transducers, the structure was then bonded onto a glass slide base. This also allowed for bottom-illumination during imaging of aligned patterns. Wire leads were soldered on the transducer electrodes using lead free solder (Steiner & Martins Inc.). The other ends of the wires were connected in parallel to the output of a high frequency RF Amplifier (240L, E&I Ltd.). A function generator (33500b, Keysight) was used to generate the input signal, which upon amplification, actuated the piezo transducers.

3.3 Determining the Effect of Ultrasound Actuation Parameters on Micro-particle Alignment Characteristics

To assess the effect of ultrasound frequency on the distance between adjacent strands of aligned micro-particles (referred to as inter-strand spacing henceforth), each testing fixture was set up on the stage of a top-down microscope (M83EZ-C03S, Omax Inc) with bottom illumination. A 1 ml of micro-particle suspension was pipetted out into the

testing fixture chamber. Since only one sine wave frequency can be generated at a time by the function generator, the experiments were performed one testing fixture (implying 1 MHz, 1.5 MHz, 2 MHz or 3MHz) at a time. At each frequency, the experiments were performed at two peak to peak voltages of the AC sine wave, 80 mVpp and 160 mVpp, to determine the effect of pressure amplitude on the inter-strand spacing. To prevent overheating and damage to the transducers, burst mode of excitation was utilized, wherein the transducers were excited for a period of 2 seconds, followed by a resting period of 0.5 seconds. The total burst mode excitation duration in each experiment was 60 s. The experiments at each frequency and amplitude level were performed in triplicate. The images (4X mag) were analyzed in NIH ImageJ software [16] to determine the inter-strand spacing between aligned micro-particle strands. The values are reported as mean ± standard deviation of measurements taken at ten random locations from each image. Two-way ANOVA was then performed ($\alpha = 0.05$) with measured inter-strand spacing as the dependent variable, and frequency and amplitude as two independent factors having four and two levels, respectively.

4. Results and Discussion

Actuation of the transducers caused them to vibrate along their thickness, thereby creating a standing acoustic wave within the water, with pressure nodes co-planar to the walls of the transducers. The polymer micro-particles slowly migrated to the nearest pressure node, acted upon by the ensuing ARF. These pressure nodes are planes parallel to the walls of the transducers (Figure 1a). Figure 2 demonstrates how the micro-particles migrated over time to aggregate into distinct strands over the 60 s duration.

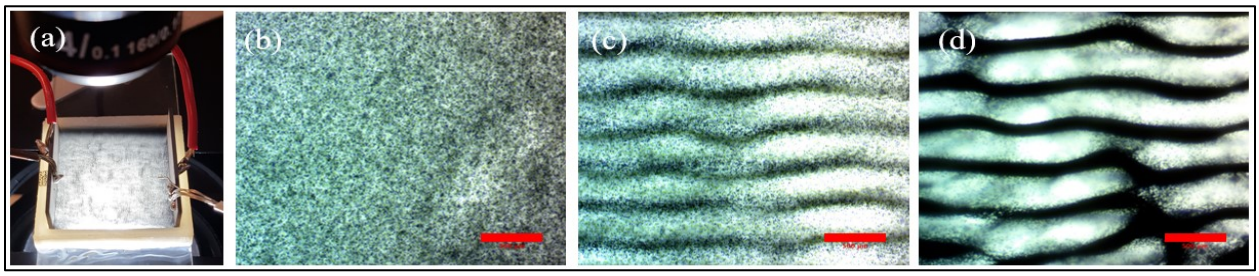

Figure 2: Alignment of polyethylene micro-particles in the experimental setup (a) for 3MHz transducers over time. Images (b), (c) and (d) were taken at 4X magnification at time points 0, 30 and 60 s respectively. Scale bar = 500 µm

Figures 3 and 4 show how increasing frequency resulted in smaller inter-strand spacing at the end of 60 s ($p < 0.001$). Increasing the voltage amplitude reduced the time taken to align the particles, but the resulting inter-strand spacings were not statistically different ($p = 0.471$). Moreover, the observed spacings were noticeably larger than the theoretical spacings ($\lambda/2$) between adjacent pressure nodes (Equation (1)) at all four frequencies and both amplitudes. This difference can be attributed to the compliance of the transducers to the input signal, wherein the actual vibration frequencies of two transducers with the same frequency rating may be slightly different from each other due to material and process associated variabilities. Another reason is the acoustic streaming effect, which is caused due to high amount of displacement created within the transducers at the resonant frequency. This effect was especially evident at 160 mVpp for 1 MHz transducers, wherein high amount of turbulence destroyed any alignment, and hence, the result has not been reported, and the corresponding value for 80mVpp not used in the two-way ANOVA. Alignment was also slightly disturbed by the burst mode of excitation. Sudden actuation after the resting period in the burst mode causes minor turbulence within the testing chamber, which may displace the particles resulting in aberrations in particle clustering.

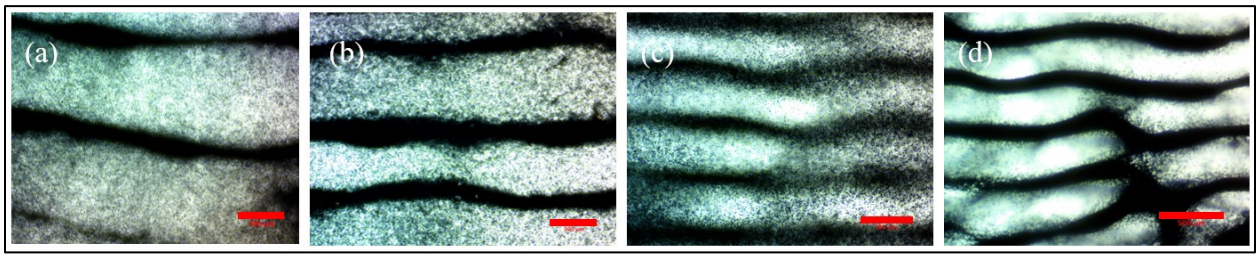

Figure 3: Alignment of polyethylene micro-particles after 60 s of excitation at 80 mVpp for (a) 1 MHz, (b) 1.5 MHz, (c) 2 MHz, and (d) 3 MHz. Scale bar = 500 µm. For all frequencies, the inter-strand spacings observed at 160 mVpp were not statistically different from the spacings at 80 mVpp ($p > 0.05$).

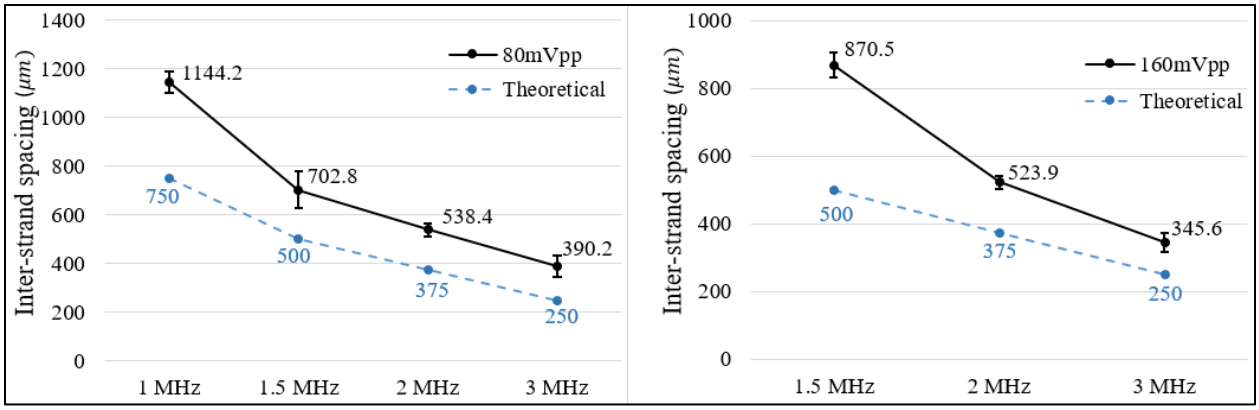

Figure 4: Observed and theoretical inter-strand spacings at each frequency and excitation voltage. The inter-strand spacing was inversely proportional to the frequency, but it was larger than the theoretical estimate in all cases. Coherent alignment was not observed for 1 MHz at 160 mVpp due to significant acoustic streaming.

From Equation (4), it is evident that for this micro-particle suspension in water: 1) ARF is directly proportional to frequency, 2) ARF is independent of the viscosity of the fluid [14], 3) larger particles experience significantly greater ARF than smaller particles, and 4) small increases in the pressure amplitude (resulting from increases in Vpp) result in higher ARF. Considering a typical pressure amplitude of 100 kPa as has previously been described [18], compressibility of water and toner particles as 456 TPa^{-1} and 100 TPa^{-1}, respectively [17], and speed of sound in water (1500 m/s), the ARF acting on the micro-particles at 1 MHz is approximately 800 nN (calculated from Equation (4)). Although the magnitude of ARF is so small, it is higher than the maximum fluid resistive force estimate of approximately 450 nN (calculated from Equation (5)), causing the particles to move. Note that 100 kPa pressure is used in these calculations as a representative scenario based on literature [18]. The amount of pressure being generated by a particular voltage amplitude could be more closely estimated by finite element modelling of the piezo-transducers coupled with a fluid, or by measurement through a sensor within the chamber.

The results above demonstrate the proof of concept of manipulating micro-particles using ultrasound. The fluid matrix in actual engineering applications will most likely not be water but some functional photonically or chemically cross-linkable polymers with viscosities of 50 cP or higher. For these polymers, although the ARF on suspended particles would not increase, the resistive force would increase, causing a greater impediment for particles to arrange at the nodes, and requiring higher pressure amplitude (higher Vpp) for alignment. For example, hydrogels, such as alginate, are used in biofabricating engineered tissues and organs [19]. Living cells (equivalent of micro-particles) are encapsulated within the hydrogel, which is chemically crosslinked after a structure with the desired geometry is fabricated. Figure 5 shows results from an experiment in which human adipose derived stem cells (hASC; mean Ø 22 µm) were aligned in 2% w/v alginate (viscosity = 200 cP) using the 2 MHz piezo-transducer experimental chamber at 100 mVpp and crosslinked with 1% w/v $CaCl_2$. Upon assessment of viability via Live/Dead cell assay, 100% of the hASC were found to be viable, bolstering the reliability of such a technique to successfully pattern cells within biopolymers. This could open-up new horizons for creating highly aligned anisotropic constructs for tissues such as ligaments and tendons in which the uniaxial alignment of cells and resulting ECM is critical to the tissues' functions.

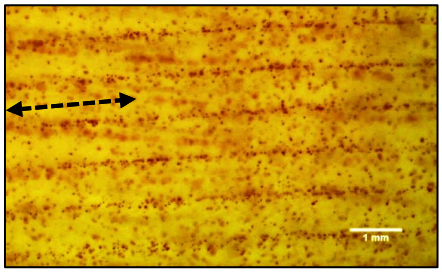

Figure 5: Alignment of living hASC (stained red) in 2% w/v alginate using the 2 MHz testing set up. The dotted arrow depicts the alignment direction. The mean observed inter-strand spacing was 410 µm, which varied from the theoretical 375 µm. Scale bar = 1 mm.

5. Conclusion

This study demonstrates a new approach for patterning micro-particles in fluid matrices to create structurally anisotropic constructs. The equation for the pressure variation within the standing wave field was derived and the corresponding expression for ARF was determined. Case-specific calculations for the ARF on a particle, and fluid resistive force it must overcome while migrating to the nodes, were performed. Experimentally, the spherical polyethylene micro-particles, which served as a cost-effective alternative to demonstrate proof of concept, could be aligned in linear strands at the coplanar pressure nodes of the standing wave field within water due to the ARF generated from the standing BAW from an opposing pair of piezo-transducers. Although the measured inter-strand spacing in each case was not equal to half the wavelength as per theory, it was inversely proportional to the excitation frequency. Also, although increasing pressure amplitude could visibly create faster alignment, it also increased turbulence in low frequency transducers, leading to incoherent alignment in some cases. The aligning of living human stem cells in a viscous hydrogel was also successfully demonstrated. This process can be further developed in future to fabricate anisotropic composites for various applications including tissue engineering.

Acknowledgement

This study was supported by a grant from the National Science Foundation (CMMI#1652489). The authors thank Brent Goldstein (North Carolina State University) for help with the ImageJ analysis.

References

1. Gibson, L. J. (2012). The hierarchical structure and mechanics of plant materials. *Journal of the Royal Society Interface*, rsif20120341.
2. Gibson, L. J., & Ashby, M. F. (1999). *Cellular solids: Structure and Properties*. Cambridge University Press.
3. Bourget, J., Guillemette, M., Veres, T., Auger, F., & Germain, L. (2013). Alignment of cells and ECM within tissue-engineered substitutes. In *Advances in Biomaterials Science & Biomedical Applications*. InTech.
4. Mauck, R. L., Baker, B. M., Nerurkar, N. L., Burdick, J. A., Li, W. J., Tuan, R. S., & Elliott, D. M. (2009). Engineering on the straight and narrow: the mechanics of nanofibrous assemblies for fiber-reinforced tissue regeneration. *Tissue Engineering Part B: Reviews*, *15*(2), 171-193.
5. Zok, F. W., Rathbun, H., He, M., Ferri, E., Mercer, C., McMeeking, R. M., & Evans, A. G. (2005). Structural performance of metallic sandwich panels with square honeycomb cores. *Philosophical Magazine*, *85*, 3207-3234.
6. Banhart, J., Baumeister, J., & Weber, M. (1996). Damping properties of aluminium foams. *Materials Science and Engineering: A*, *205*(1-2), 221-228.
7. Mallick, P. K. (2007). *Fiber-reinforced Composites: Materials, Manufacturing, and Design*. CRC Press.
8. Wong, K. V., & Hernandez, A. (2012). A review of additive manufacturing. *ISRN Mechanical Engineering*, *2012*.
9. Zhong, W., Li, F., Zhang, Z., Song, L., & Li, Z. (2001). Short fiber reinforced composites for fused deposition modeling. *Materials Science and Engineering: A*, *301*(2), 125-130.
10. Compton, B. G., & Lewis, J. A. (2014). 3D-printing of lightweight cellular composites. *Advanced Materials*, *26*(34), 5930-5935.
11. Chang, R., Nam, J., & Sun, W. (2008). Effects of dispensing pressure and nozzle diameter on cell survival from solid freeform fabrication–based direct cell writing. *Tissue Engineering Part A*, *14*(1), 41-48.
12. Nair, K., Gandhi, M., Khalil, S., Yan, K. C., Marcolongo, M., Barbee, K., & Sun, W. (2009). Characterization of cell viability during bioprinting processes. *Biotechnology Journal*, *4*(8), 1168-1177.
13. Kinsler, L. E., Frey, A. R., Coppens, A. B., & Sanders, J. V. (1999). Fundamentals of acoustics. 4th Edition, pp. 560. ISBN 0-471-84789-5. *Wiley-VCH*.
14. Yosioka, K., & Kawasima, Y. (1955). Acoustic radiation pressure on a compressible sphere. *Acta Acustica united with Acustica*, *5*(3), 167-173.
15. Odar, F., & Hamilton, W. S. (1964). Forces on a sphere accelerating in a viscous fluid. *Journal of Fluid Mechanics*, *18*(2), 302-314.
16. Rasband, W. S. (2007). ImageJ, US National Institutes of Health. *http://rsb. info. nih. gov/ij/(1997-2007)*.
17. Landau, L. D. (1959). Em lifshitz fluid mechanics. *Course of Theoretical Physics*, *6*.
18. Barnkob, R., Augustsson, P., Laurell, T., & Bruus, H. (2010). Measuring the local pressure amplitude in microchannel acoustophoresis. *Lab on a Chip*, *10*(5), 563-570.
19. Narayanan, L., Huebner, P, Fisher, M. B., Spang, J. T., Starly, B., Shirwaiker, R. A. (2016). 3D-Bioprinting of PLA Nanofiber-Alginate Hydrogel Bioink Containing Human Adipose-Derived Stem Cells. *ACS Biomaterials Science & Engineering*. 2(10): 1732-1742.